Clays and Clay Minerals, Vol. 67, No. 4:315–324, 2019

SIMULTANEOUS IMMOBILIZATION OF ZN(II) AND CR(III) IN SPINEL CRYSTALS FROM BENEFICIAL UTILIZATION OF WASTE BROWNFIELD-SITE SOILS

Fei Wu[1,2,3], Yuanyuan Tang[4], Xingwen Lu[5], Chengshuai Liu[1,2]*, Yahui Lv[2], Hui Tong[2], Zengping Ning[2], Changzhong Liao[2], and Fangbai Li[2]

[1]State Key Laboratory of Environmental Geochemistry, Institute of Geochemistry, Chinese Academy of Sciences, Guiyang 550081, China
[2]Guangdong Key Laboratory of Integrated Agro-Environmental Pollution Control and Management, Guangdong Institute of Eco-Environmental Sciences & Technology, Guangzhou 510650, China
[3]University of Chinese Academy of Sciences, Beijing 100049, China
[4]School of Environmental Science and Engineering, Southern University of Science and Technology, Shenzhen 518055, China
[5]Research Centre for Environmental Health and Pollution Control, School of Environmental Science and Engineering, Guangdong University of Technology, Guangzhou 510006, China

Abstract—Waste brownfield-site soils contaminated with heavy metals such as Zn and Cr are of critical environmental concern because of the rapid urbanization and industrialization that is occurring in China. Thermal treatment can fix heavy metals in specific mineral structures, which might be a promising technology for remediation and reutilization of the metal-contaminated soils. The objective of the present study was to elucidate the stabilization mechanisms of Zn and Cr through thermal treatment of mixtures of ZnO + Cr_2O_3 to form $ZnCr_2O_4$ and to confirm that Zn and Cr were incorporated simultaneously into the spinel structure. The incorporation efficiency for Zn was quantified, with the value ranging from 70.6 to 100% over the temperature range 700–1300°C. Leaching results further confirmed that $ZnCr_2O_4$ spinel was a superior product for Zn and Cr immobilization. Then, by artificially sintering Zn- and Cr-enriched soils, both Zn and Cr were immobilized effectively (with three orders of magnitude reduction in Zn leachability) in the $ZnCr_2O_4$ spinel as the predominant product phase. In addition, multiple heavy metals such as Zn, Cu, and Cr in the actual brownfield-site soils were well immobilized after sintering, which confirmed the potential for practical application of the thermal treatment technology utilized in this study.

Keywords—Brownfield site soils · Chromium · Simultaneous immobilization · Spinel · Thermal treatment · Zinc

INTRODUCTION

With rapid urbanization and industrialization in China, many old factories have been or are being relocated or closed, leaving underutilized and abandoned land as brownfield sites which were heavily contaminated by the industrial activities (Woetzel et al. 2009; Coulon et al. 2016). The high levels of pollutants in the soils of brownfield sites mean that considerable remediation is necessary before the former industrial sites can be brought back into beneficial use (Chen et al. 2009; Bardos et al. 2016). Hazardous metals in the site soils are usually from industrial emissions, traffic emissions, and mining activities (Luo et al. 2012; Li et al. 2013, 2018). The main heavy metals include lead (Pb), arsenic (As), mercury (Hg), zinc (Zn), cadmium (Cd), copper (Cu), nickel (Ni), and chromium (Cr) (De Kimpe & Morel, 2000; Gallagher et al. 2008; Wuana & Okieimen, 2011). Hazardous metals are non-biodegradable and thus persistent in soils, which not only affects the yield and quality of farm crops, but also causes direct health injury to human beings living on brownfield sites (Prabhukumar et al. 2004; Fu et al. 2012). Effective and economical remediation technologies, therefore, should be taken into account to eliminate the environmental risks before redeveloping contaminated sites.

Currently, a large number of techniques has been applied for the remediation of heavy-metal-contaminated brownfield-site soils (Huynh et al. 2003; Dermont et al. 2008; Yao et al. 2012; Cameselle & Gouveia 2019). For example, soil washing, excavation, transport, and landfilling can remove metal pollutants from the sites, but these methods are difficult to apply on a large scale due to the potential for secondary pollution, the significant operation cost, and the limited number of landfills (Basta & McGowen, 2004; Lee et al. 2009). Another remediation approach for contaminated sites is the in situ stabilization/solidification (S/S) method, which can reduce the bioavailability of heavy metals by immobilization agents or amendments (Lee et al. 2009; Bolan et al. 2014; Sun et al. 2015; Capobianco et al. 2017). In the traditional S/S method, however, the heavy metals are stabilized only by sorption or weak chemical bonds, which means they may be further released into the medium and may

Fei Wu and Yuanyuan Tang contributed equally to this work.

This paper was originally presented during the World Forum on Industrial Minerals, held in Qing Yang, China, October 2018

Electronic supplementary material The online version of this article (https://doi.org/10.1007/s42860-019-00053-w) contains supplementary material, which is available to authorized users.

* E-mail address of corresponding author: liuchengshuai@vip.gyig.ac.cn
DOI: 10.1007/s42860-019-00053-w

persist for long periods, especially when the soils are acidified (Tang et al. 2011a, b; Velasco et al. 2014).

Based on phase transformation during ceramic sintering, hazardous metals can be incorporated into some specific crystal structures after interacting with the major components in the ceramic matrices (Tang et al. 2016). Spinel has been recognized as a promising phase in which a variety of metals like Zn, Cu, and Cd may be stabilized. Spinel is usually expressed with the general formula of "AB_2O_4", where "*A*" represents divalent metals such as Zn, Cu, or Cd, and "*B*" represents trivalent matrix metal element such as Al and Fe (Marinković et al. 2004). For example, by sintering ZnO with Al-containing ceramic materials, Zn was stabilized successfully by being incorporated into a $ZnAl_2O_4$ spinel structure (Tang et al. 2011a, b, 2016; Tang & Shih 2014). Other studies also reported the transformation of Cu, Ni, and Cd into their corresponding spinel structures by sintering with Al-rich ceramic precursors (Shih et al. 2006; Tang et al. 2011a, b, 2014; Lu & Shih 2012; Mao et al. 2014; Su et al. 2017). The studies mentioned above, however, focused mainly on the potential of using Al as the "*B*" ion in order to incorporate the divalent heavy metals into the "*A*" site; whereas, in actual brownfield-site soils the hazardous metals usually coexist together due to the diversity of metals released during the industrial activities on/around the sites (Fonseca et al. 2011). In contrast to having only a single type of metal, the coexistence of multiple metals in the soils may cause interactive behavior and combined ecological effects, thus making soil remediation much more challenging (Lombi et al. 2001). Considering the reality of contaminated soils on brownfield sites as containing various metals with different properties, studies of potential strategies to achieve the simultaneous immobilization of different metals are important and urgent.

Among the hazardous metals found in brownfield-site soils, Cr and Zn are of most concern and in need of immobilization (Mulligan et al. 2001; Li et al. 2014; Zhou et al. 2017). Chromium usually in two oxidation states (Cr(III) and Cr(VI)), Cr(III) being the preferred state because it is less mobile and less toxic (Hsu et al. 2009). When divalent Zn coexists with trivalent Cr, both are expected to be incorporated into the spinel structure upon heating. The purpose of the present study, therefore, was, firstly: to determine whether a mixed-metal system of ZnO and Cr_2O_3 could be crystallized together through a sintering process; secondly: to clarify whether the same incorporation mechanisms would work in a simulated brownfield soil contaminated by both Zn and Cr; and thirdly: to utilize the technology with an actual brownfield soil to confirm that it is suitable for field application. By choosing Zn and Cr as two target metals, this study intended to propose a strategy for the simultaneous immobilization of multiple hazardous metals by incorporating them into stable crystal structures based on their specific properties, and finally to develop a "waste-to-resource" approach for the safe and beneficial utilization of metal-containing solid wastes, such as the brownfield-site soils, in the form of ceramic materials.

MATERIALS AND METHODS

Sample Preparation

Three series of samples were prepared for the study, including simple mixture of ZnO and Cr_2O_3 (ZC series), artificially Zn- and Cr-enriched soils (AZC series), and actual brownfield-site soils (ASS series). The ZnO and Cr_2O_3 powders were purchased from Sigma Aldrich Co. (St. Louis, Missouri, USA), and then mixed to prepare the ZC series with a total dry weight of 100 g at a molar ratio of Zn:Cr = 1:2. The AZC series was prepared by adding 10 g of the ZnO + Cr_2O_3 mixture (Zn:Cr molar ratio of 1:2) to 90 g of uncontaminated soil collected from Hunan Province, China. A bulk soil sample of ~20 kg was collected from a depth of 0–20 cm during the summer of 2017. The soils collected were air dried and then ground to pass through a 2-mm sieve. In addition, the ASS samples were collected from a contaminated site in Hunan Province, China, which has been used as a smelting plant for ~50 years. Again, a bulk soil sample of ~20 kg was collected from a depth of 0–20 cm in 2017. The soils collected were air-dried for a week and passed through a 13 mm sieve after careful removal of crop residues and other non-soil materials. About 1.5 kg of subsample was taken from the bulk sample after thorough mixing and was then ground to pass a 2 mm sieve.

The mixing process was carried out by ball milling the powder in a water slurry (100 g powder with 100 mL water) for 18 h. The ball milling was conducted in a planetary mill machine with four agate grinding jars (500 mL each) at a rotation speed of 180 rpm. The slurry samples were then dried in the oven at 105°C for 24 h and further homogenized by extended mortar grinding for 10 min by hand with an agate mortar and pestle. The powder mixture was pressed into pellets with a 20 mm diameter to ensure consistent compaction of the powder samples for the sintering process. Each pellet was pressed from 3 g of the powder mixture under a pressure of 320 MPa with holding time of 1 min. After that, the sample pellets were submitted to a controlled sintering scheme at target temperatures ranging from 700°C to 1300°C and a dwell time of 3 h, with controlled heating and cooling rates of 10°C/min. After this thermal treatment, the pellets were cooled in ambient air to room temperature.

Sample Characterization

The metal contents of the collected soils were measured using an AX-PETRO X-ray fluorescence spectrometer (XRF, PANalytical, Almelo, The Netherlands). After the sintering process, each pellet sample was ground into a fine powder, giving a particle size <45 μm, and then analyzed by X-ray diffraction (XRD). The XRD pattern of each powder sample was collected using a Philips-X'Pert Pro MPD (PANalytical, Almelo, The Netherlands) equipped with a Cu tube ($K\alpha_{1,2}$, λ = 1.54059 Å), operating voltage of 40 kV and current of 40 mA, and an X'celerator detector. The scanning angle range was 10 to 90°2θ with a step size of 0.02°2θ and a scanning speed of 0.5 s per step. To monitor the phase transformation, the diffraction patterns collected were analyzed by matching

https://doi.org/10.1007/s42860-019-00053-w Published online by Cambridge University Press

with standard powder diffraction patterns from the International Centre for Diffraction Data (ICDD PDF-2 Release 2008).

X-ray photoelectron spectroscopy (XPS) analysis was performed using an ESCALAB 250 Xi photoelectron spectrometer (Thermo Fisher Scientific, Waltham, Massachusetts, USA) with Al Kα X-rays as the source (1486.6 eV) at 20 kV. The basic vacuum during analysis was ~ 2×10^{-7} Pa, and the binding energy (BE) scales for the samples were referenced by setting the adventitious carbon C(1s) peak to 285 eV (Naumkin et al. 2008). The BEs were measured with a precision of ±0.2 eV. The high-resolution C(1s), Zn(2p), Cr(2p), and O(1s) spectra were obtained at a pass energy of 50 eV. The samples in powder form were pressed into pellets 1 mm thick and 1 cm in diameter before being introduced into the ultrahigh vacuum. The XPS peaks with multiple components were resolved by the peak-fitting program *XPSPEAK*4.1 assuming 100% Gaussian peak shape.

Transmission electron microscopy (TEM) analysis was conducted using a JEM-2100F electron microscope (JEOL, Tokyo, Japan), equipped with energy dispersive X-ray spectroscopy (EDS). Samples for TEM were prepared by sonicating 10 mg of the powder in 10 mL of ethanol for 1 h and then depositing a few drops of the suspension on a Cu grid coated with a holey carbon film. Moreover, X-ray absorption near-edge structure (XANES) spectra were used to determine the oxidation state/speciation of Cr and the adjacent local structure. The Cr K-edge (5989 eV) XANES spectra were collected in transmission mode using a Lytle detector at the 16 A beamline of NSRRC (Hsinchu, Taiwan). The spectra of the pure chemicals of Cr_2O_3 and CrO_3 were also measured as reference for Cr(III) and Cr(VI) oxidation states. Powders were fixed on a thin film (XRF tape) and covered with a 4 μm thick Ultralene film (SPEX CertiPrep, Metuchen, New Jersey, USA). XANES spectra were recorded between 5.96 and 6.21 keV with a step of 0.2 eV and a cumulative time of 1 s/step. The XANES data processing and analysis were carried out using *ATHENA* (Demeter software package version 0.9.18).

Leaching Experiments

The samples for leaching experiments were prepared by breaking and grinding the pellets, as obtained above, into a fine powder (<0.45 μm). The metal leachability was tested by a leaching procedure modified from the U.S. EPA Toxicity Characteristic Leaching Procedure (TCLP) with acetic acid solution (extraction fluid #2, pH ~ 2.9) as the leaching fluid (USEPA, Method 1311). Each leaching vial was filled with 10 mL of TCLP extraction solution and 0.5 g of sample powder. The leaching vials were rotated end-over-end at 30 rpm for agitation periods from 0.75 to 21 days. At the end of each leaching test, the leachates were filtered through 0.25 μm cellulose membranes (Jinteng Co., Ltd., Tianjin, China). The pH of the filtrates was measured, and the concentrations of Zn and Cr were determined using an inductively coupled plasma optical emission spectrometer (ICP-OES Optima 8000, PerkinElmer, Waltham, Massachusetts, USA). All the above-mentioned leaching procedures for each sample were performed in triplicate to ensure reproducibility.

RESULTS AND DISCUSSION

Formation of the $ZnCr_2O_4$ Spinel from ZnO and Cr_2O_3

Phase Transformation of Zn- and Cr-Containing Compositions Based on the hypothesis for AB_2O_4 spinel formation, the molar ratio of Zn as divalent ion to Cr as trivalent ion was set at 1:2, which is stoichiometrically consistent with the ratio of the two metals in the product phase. From the XRD patterns of the sintered ZC sample series after thermal treatment at 700–1200°C (Fig. 1), the initial crystal phases were identified as ZnO (PDF #89-7102) and Cr_2O_3 (PDF #04-0765). The formation of the $ZnCr_2O_4$ spinel (PDF #87-0028) was first detected in the sample sintered at 700°C. In the initial stage of the spinel phase ($ZnCr_2O_4$) formation, a solid-state reaction occurred between the ZnO and Cr_2O_3 due to a nucleation process, subsequently leading to the formation of spinel $ZnCr_2O_4$ with a cubic face structure (Dixit et al. 2015). The potential reaction between ZnO and Cr_2O_3 is expressed as:

$$\mathrm{ZnO(orthorhombic) + Cr_2O_3(orthorhombic) \rightarrow ZnCr_2O_4(octahedron)} \quad (1)$$

With increase of sintering temperature, a substantial increase in the intensity of the $ZnCr_2O_4$ peaks was observed, together with a simultaneous decrease in the peaks of ZnO and Cr_2O_3. At 1000°C, no peaks of ZnO and Cr_2O_3 could be identified after 3 h of sintering, implying complete transformation of both reactants. Subsequently, the diffraction peaks of the $ZnCr_2O_4$ were sharper and narrower as the sintering temperature increased, which indicated enhancement of the crystalline phase due to the enlargement of the particles (Gene et al. 2015).

As Zn and Cr are mixed stoichiometrically in the reaction system, the transformation efficiency for either of the two metals is reflected by their incorporation into the spinel structure. Therefore, a "transformation ratio (*TR*, %)" index was defined as below, based on the quantification results of all Zn-containing components in the reaction system:

$$TR = \left(\frac{\mathrm{wt.\%\,of\,ZnCr_2O_4}}{\mathrm{MW\,of\,ZnCr_2O_4}}\right) \Big/ \left(\frac{\mathrm{wt.\%\,of\,ZnCr_2O_4}}{\mathrm{MW\,of\,ZnCr_2O_4}} + \frac{\mathrm{wt.\%\,of\,ZnO}}{\mathrm{MW\,of\,ZnO}}\right) \quad (2)$$

where MW refers to the molecular weight. A *TR* value of 100% implies complete transformation of Zn and Cr into the $ZnCr_2O_4$ spinel structure.

From the *TR*s summarized in Fig. 2, 70.55% of Zn was transformed into the $ZnCr_2O_4$ structure even at the lowest temperature in the thermal treatment used in this study. With further increase in the sintering temperature, the *TR* value of Zn increased continuously until reaching nearly full incorporation (*TR* = 100%) at 1300°C. The driving forces for mass transfer

https://doi.org/10.1007/s42860-019-00053-w Published online by Cambridge University Press

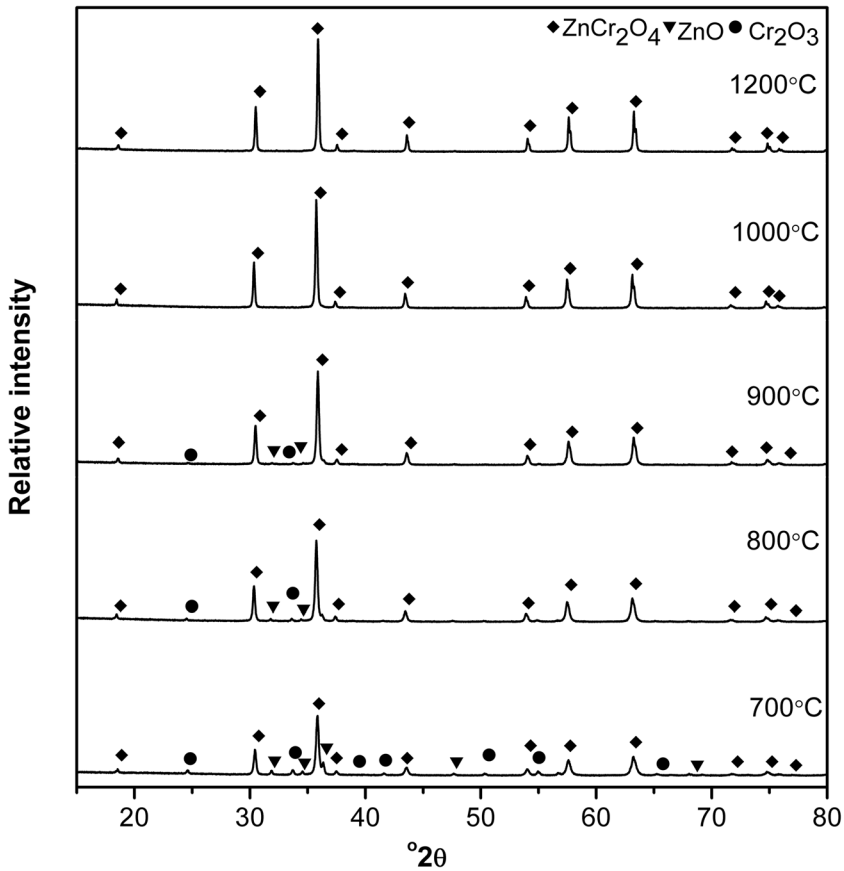

Fig. 1 XRD patterns of sintered ZnO + Cr_2O_3, at 700 to 1200°C for 3 h. The standard patterns retrieved from the ICDD database included ZnO (PDF #89-7102), Cr_2O_3 (PDF #04-0765), and $ZnCr_2O_4$ (PDF #87-0028)

during thermal treatment are the differences in chemical potential (free enthalpy or molar Gibbs free energy) among the firing materials (Sarıkaya et al. 2008). The value of $\Delta_r G$ (standard Gibbs free energy) for the reaction between ZnO and Cr_2O_3 at 1000 K is –88.06 kJ mol^{-1}, leading to the efficient transformation of Zn and Cr into the $ZnCr_2O_4$ spinel at a relatively lower temperature (Stephen et al. 2007).

Incorporation Mechanisms of Zn and Cr into $ZnCr_2O_4$ Spinel The XPS spectra of the products obtained through sintering the mixture of ZnO + Cr_2O_3 at 1000°C for 3 h are shown in Fig. 3. A full-scan XPS spectrum (Fig. 3a) was analyzed to study the surface elemental composition of the sample measured. To compensate for the shift in energy due to surface charging, the observed binding energies were all adjusted by assigning the main C 1s peak to 284.8 eV (adventitious carbon). In the XPS survey spectrum of the sample sintered at 1000°C, various peaks were observed corresponding to Zn 2p1/2 (1044.8 eV), Zn 3s (139.8 eV), Zn 3p (89.8 eV), Zn 2p3/2 (1021.8 eV), Cr 3p (61.4 eV), Cr 2p (611.0 eV), and O 1s (530.8 eV). To examine the chemical states of Zn and Cr in the thermal-treated sample, the XPS narrow spectra of Zn, Cr, and O were further analyzed with Gaussian fitting. The peaks at 1021.8 eV and 1044.8 eV were attributed to the binding energies of Zn 2p3/2 and Zn 2p1/2 (Fig. 3b), the perfect symmetrical Zn 2p peaks ruled out the existence of multiple components of Zn in the samples, so Zn was expressed in the lattice in the form of Zn^{2+}. However, one cannot specify whether the Zn^{2+} ions were present in ZnO or $ZnCr_2O_4$, due to the similar XPS peak position of Zn^{2+} ions in these two phases (Song et al. 2017). Figure 3c further shows two Gaussian-fitted peaks (Cr 2p3/2 and Cr 2p1/2) at 576.7 eV and 586.1 eV, respectively, which correspond to Cr^{3+} in $ZnCr_2O_4$ (Gingasu et al. 2014). In addition, a relatively small Cr 2p3/2 peak at 575.6 eV confirmed the presence of a small amount of Cr_2O_3 on the surface of the solids obtained after thermal treatment (Epling et al. 1997). The atomic Zn/Cr ratio was 25:54 on the surface of the sintered sample, which is consistent with the atomic ratio of the $ZnCr_2O_4$ spinel which was confirmed to be the dominant state of Zn^{2+} in the near-surface region. The O 1s feature of $ZnCr_2O_4$ has a binding energy of 530.8 eV, which is consistent with the interpretation of the Zn 2p and Cr 2p spectra, indicating that $ZnCr_2O_4$ oxide is the primary state of Zn and Cr species in the near-surface region.

TEM images of the $ZnCr_2O_4$ obtained at different temperatures revealed a heterogeneous morphology of the 700°C treated sample but a more homogeneous morphology for the 1000°C and 1300°C sintered samples (Fig. 4). With the increase in the sintering temperature, the particle sizes became larger and more

https://doi.org/10.1007/s42860-019-00053-w Published online by Cambridge University Press

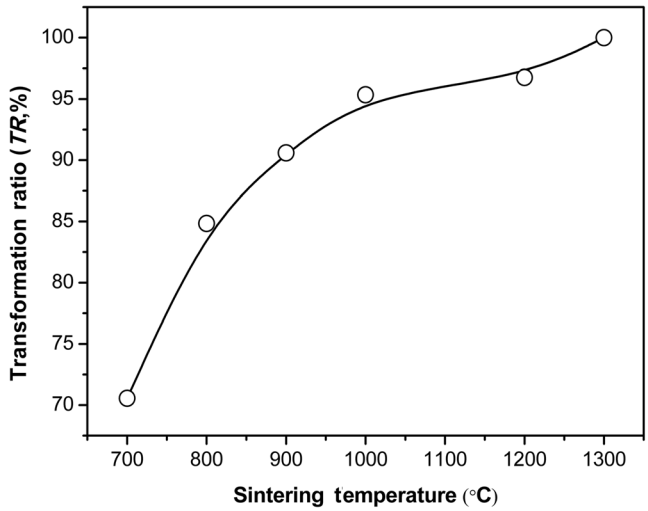

Fig. 2 The transformation ratio (*TR*, %) of Zn into the $ZnCr_2O_4$ spinel structure after sintering the mixture of ZnO + Cr_2O_3

uniform, due to the melting and fusion of adjacent particles at high temperatures (Gingasu et al. 2014). The EDX spectrum of the 1300°C sintered sample, together with the calculated atomic composition, are summarized in Fig. S1 and Table S1. The corresponding peaks of Zn, Cr, and O were observed with strong signals in the sample, and the elemental composition of

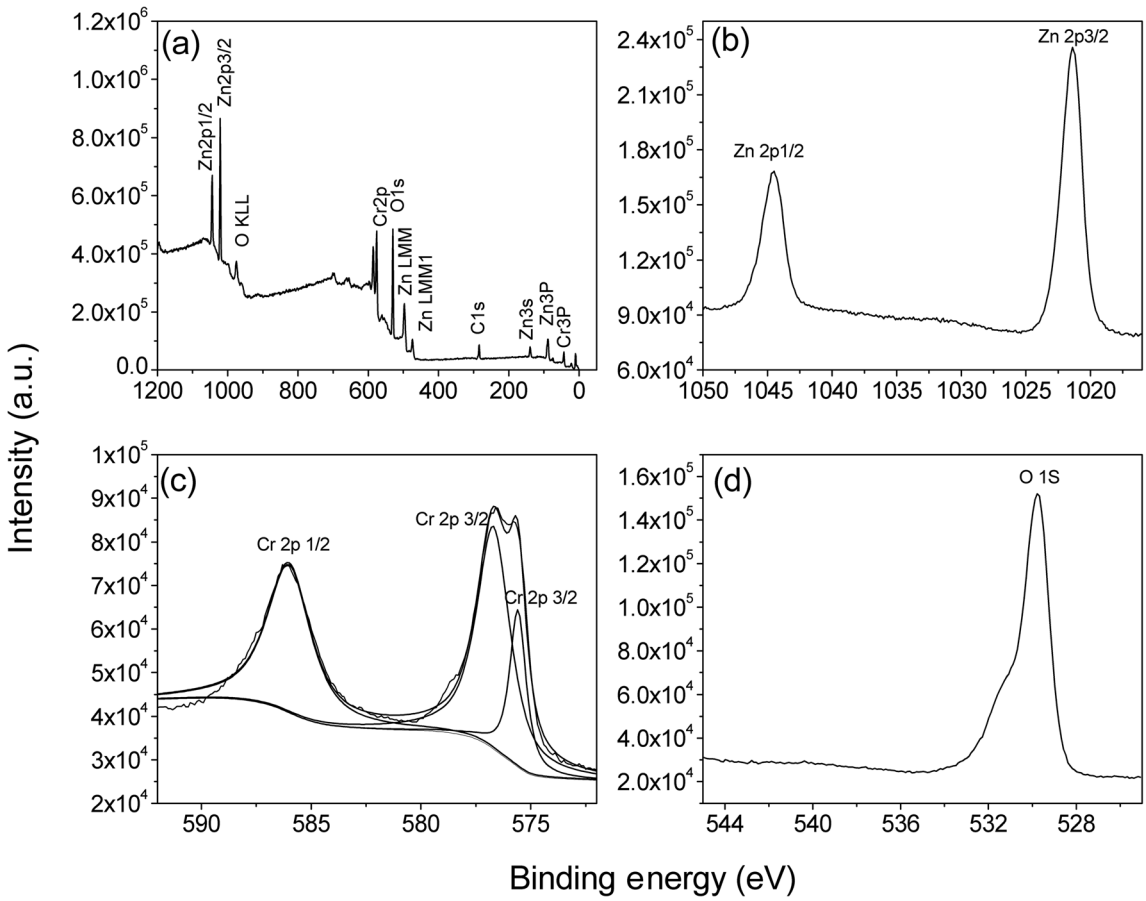

Fig. 3 (**a**) XPS survey spectrum, (**b**) XPS narrow spectrum of Zn 2p, (**c**) Cr 2p, and (**d**) O 1s of the products obtained through sintering the mixture of ZnO + Cr_2O_3 at 1000°C for 3 h

https://doi.org/10.1007/s42860-019-00053-w Published online by Cambridge University Press

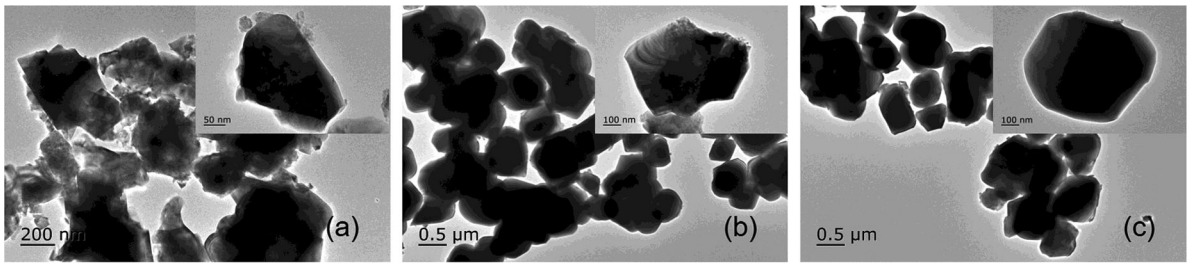

Fig. 4 TEM images of the products obtained after sintering the mixture of ZnO + Cr_2O_3 at (**a**) 700°C, (**b**) 1000°C, and (**c**) 1300°C for 3 h

Zn and Cr were 28% and 52%, respectively. Therefore, the results of EDX analysis confirmed the successful transformation of Zn and Cr into the $ZnCr_2O_4$ spinel.

The Cr K-edge XANES spectra of the samples sintered at 900°C and 1350°C, together with those of the reference compounds containing Cr(III) and Cr(VI) (Cr_2O_3 for Cr(III) and CrO_3 and $K_2Cr_2O_7$ for Cr(VI)) are shown in Fig. 5. The pre-edge feature of Cr(VI) was not observed in the sintered products, indicating that the Cr(III) in the raw materials was not oxidized to Cr(VI) during the thermal treatment processes (Lin & Wang, 2012). As shown in the insert in Fig. 5, the pre-edge peak "C" decreased while the white line peak increased in the sample obtained at the higher temperature (1350°C). As the pre-edge peak is related to the 1s to 3d quadrupole transitions, the increase of the pre-edge peak intensity can be attributed to the enhancement of the p–d orbital mixing in the tetrahedral structure. Therefore, the increase of the pre-edge peak intensity reflects the increase in the number of Cr atoms occupying the tetrahedral site (Chen et al. 2013).

Leaching Behavior of Zn and Cr from $ZnCr_2O_4$ Spinel

A prolonged TCLP leaching procedure was conducted to evaluate the stability of Zn and Cr in pure $ZnCr_2O_4$ spinel, in comparison with the corresponding metal leachability from ZnO and Cr_2O_3. Moreover, the leaching performance of the 700~1300°C-sintered sample mixture was also tested to reflect the stability of the metals in real ceramic products. The changes in concentration of Zn and Cr in the leachates of ZnO, Cr_2O_3, and pure $ZnCr_2O_4$ spinel, as well as in the sample mixture before and after sintering processes, are shown in Fig. 6. The concentration of Zn in ZnO leachate increased substantially to 1160 mg/L even after 0.75 days of leaching (inset in Fig. 6a),

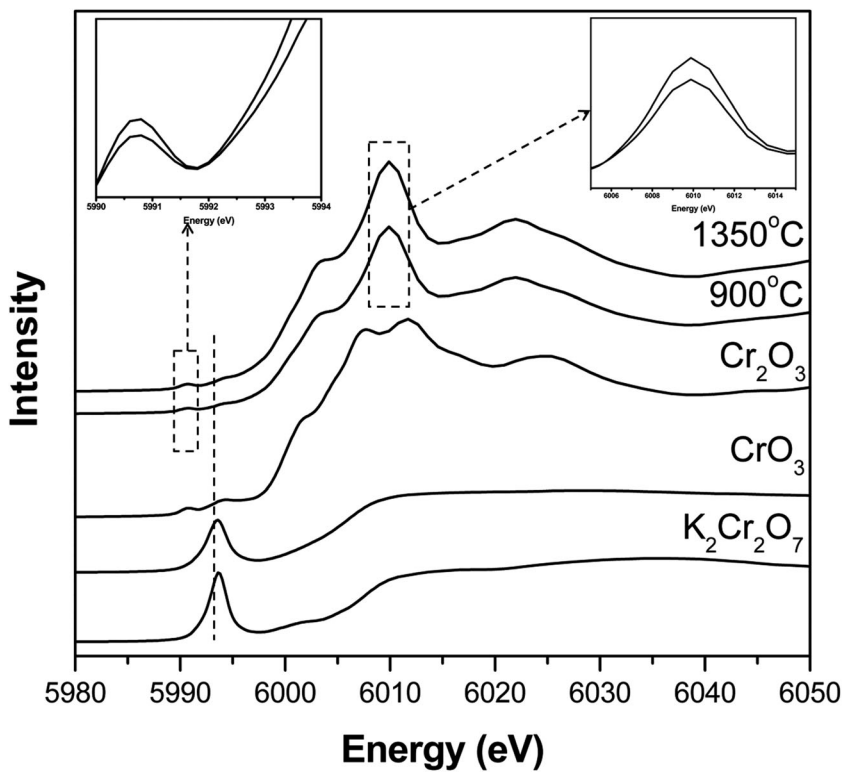

Fig. 5 Cr K-edge XANES spectra of products obtained after sintering at 900°C and 1350°C

https://doi.org/10.1007/s42860-019-00053-w Published online by Cambridge University Press

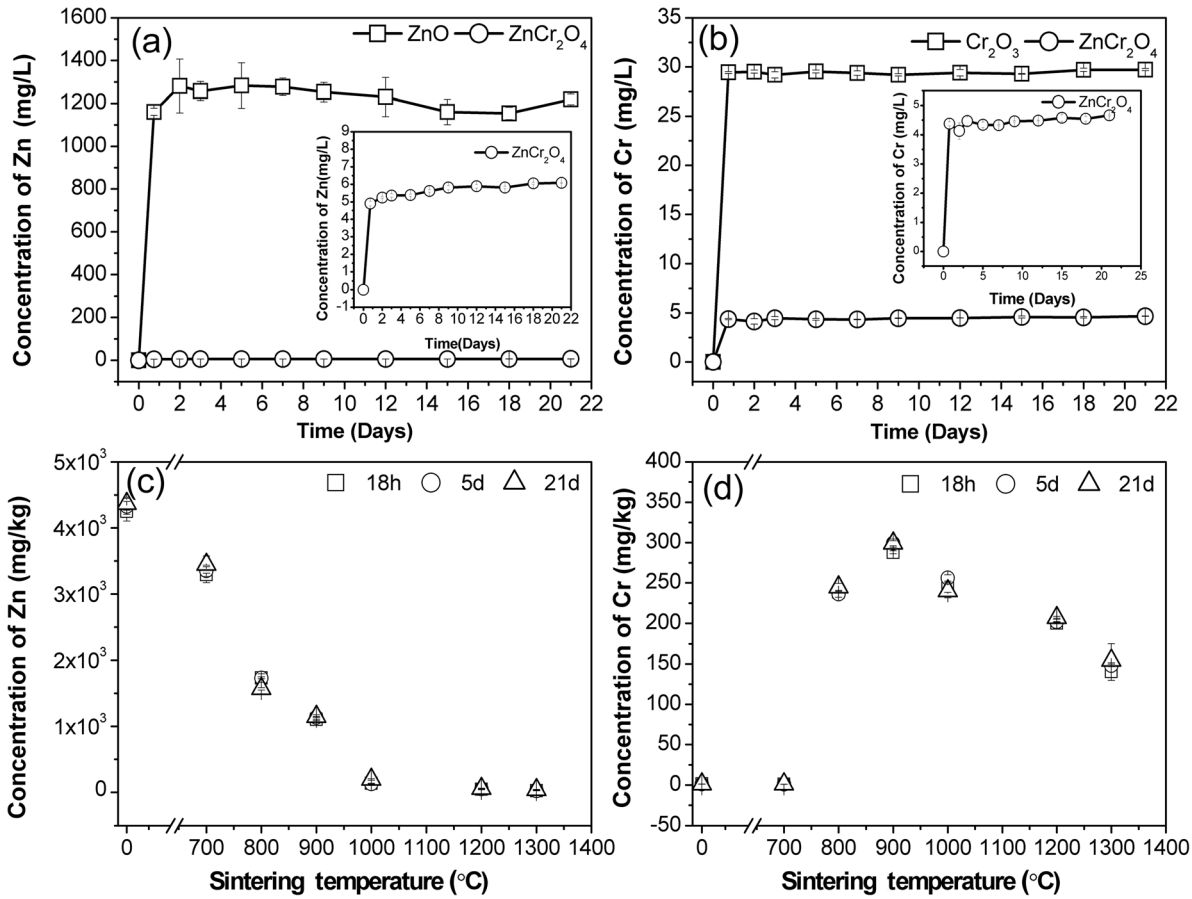

Fig. 6 The concentrations of Zn and Cr in the leachate after sample leaching with leaching periods of 0.75, 5, or 21 days. (**a**) Zn concentration as ZnO and $ZnCr_2O_4$, (**b**) Cr concentration as Cr_2O_3, (**c**) Zn, and (**d**) Cr concentrations of the mixtures after sintering at ~700–1300°C

while that value reached 29 mg/L in the leachate of Cr_2O_3 (inset in Fig. 6b). Then, the pH was ~6.4 and 3.2 for the leachates of ZnO and Cr_2O_3, respectively, while the concentration of Zn and Cr remained at 1200 and 30 mg/L,

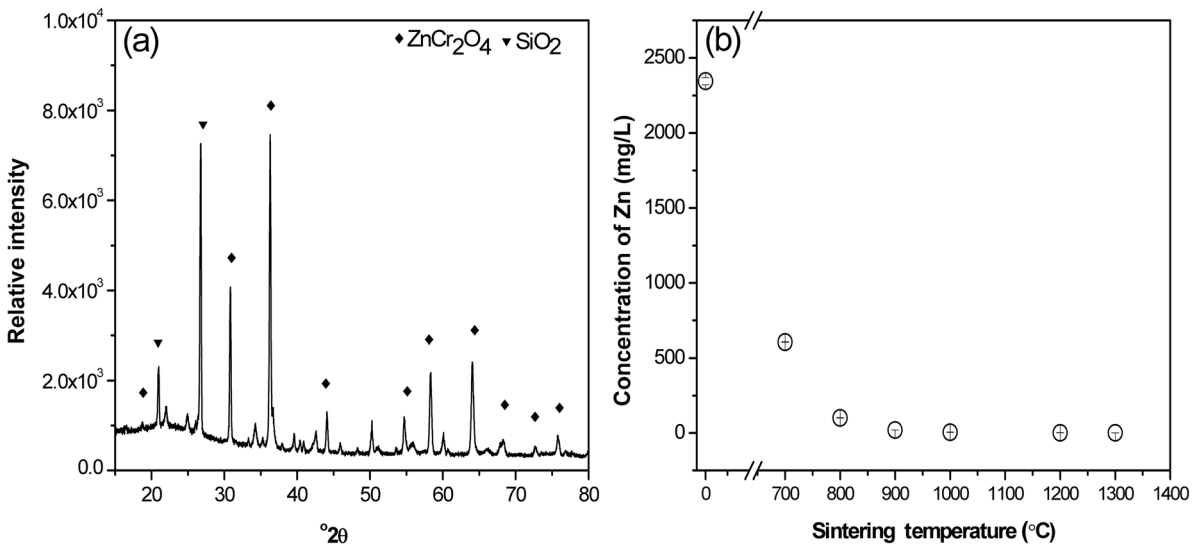

Fig. 7 (**a**) XRD pattern of the artificially Zn- and Cr-enriched soils sintered at 1000°C for 3 h, and (**b**) the Zn concentration in the 18 h leachates of the above soils sintered at temperatures from 700 to 1350°C for 3 h

https://doi.org/10.1007/s42860-019-00053-w Published online by Cambridge University Press

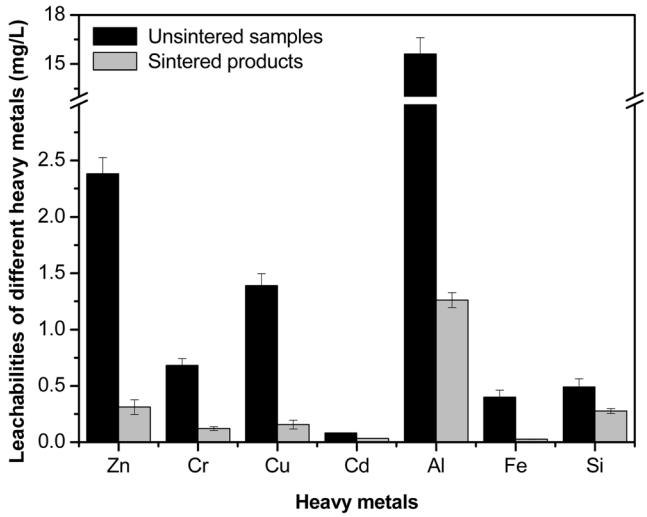

Fig. 8 Concentrations of Zn, Cr, Cu, Cd, Al, Fe, and Si in the leachates of the brownfield-site soils collected before and after sintering at 1000°C for 3 h. The initial pH value of the leaching liquid was 2.9

respectively, during the rest of the leaching period. However, for the leachate of $ZnCr_2O_4$ spinel, a dramatic decrease was detected in Zn (30 times) and Cr (5 times) concentrations compared with the leachates of their metal oxide forms (insets in Fig. 6a and 6b). With prolonged leaching, the concentrations of both metals remained at the initial value even though the pH of the leachate was very low (~3.2) until the end of this leaching experiment (Fig. S2a).

To evaluate further the stability of Zn and Cr in the sintered products, leaching experiments on the raw mixture of ZnO + Cr_2O_3 and the mixture sintered at various temperatures were performed. The amount of Zn leached from the raw mixture (Fig. 6c) reached ~2125 mg/L, but that amount decreased by a factor of three when the mixture was sintered at a relatively low temperature (800°C). Moreover, with further temperature increase, a substantial decrease was observed until reaching ~25 mg/L in the leachates of samples sintered at temperatures ≥1200°C. Proton-metal exchange is the dominant proton depletion process in the acid environment (Snellings, 2015), which results in a very high concentration of Zn in the leachates of the raw mixture and in samples treated at lower temperatures (Fig. 6c). As reflected in the pH value shown in Fig. S2a, the leachate pH was ~6.5 after leaching for 0.75 days. Therefore, the protons were completely consumed by more mobile Zn, which will inhibit the leaching of Cr, resulting in the very low concentrations (nearly zero) in the leachates of the raw mixture and samples sintered at 700°C (Fig. 6d). With the formation of $ZnCr_2O_4$ spinel, the leachability of Zn was reduced significantly due to its incorporation into the spinel structure. As a result, the extra protons in the solution attacked Cr instead and caused the Cr concentration to increase in the leachates of products sintered at 800–1000°C. With the continuous formation of $ZnCr_2O_4$ spinel, however, the leachability of Cr also decreased by >3 timeseven in an acidic environment with a pH of ~3.0. Moreover, Zn and Cr concentrations in the leachates of sintered samples were greater (Fig. 6), which further indicates the excellent performance of $ZnCr_2O_4$ spinel in long-term resistance to acidic attack.

Co-Immobilization of Zn and Cr in Actual Contaminated Soils

The above results confirmed that thermal treatment of a ZnO and Cr_2O_3 mixture successfully incorporated Zn and Cr into the stable $ZnCr_2O_4$ spinel structure, so the next step was to apply the method to waste brownfield-site soils in which Zn and Cr are both typical metal pollutants (Kumpiene et al. 2008). Results from other studies (Kadir et al. 2018; Su et al. 2018; Tang et al. 2018) also gave encouragement that such an approach would be successful in stabilizing the Zn^{2+} and Cr^{3+} ions. Those studies also indicated that the presence of Al, Si, and Fe (oxyhydr)oxides in the soils could further facilitate the stabilization of the heavy-metal pollutants. Although the waste brownfield soil is highly polluted, the Zn and Cr contents are still much lower than those of the major elements contained in the soil, such as Si, Al, and Fe (Table S2). Therefore, even with the successful incorporation of Zn and Cr into the spinel structure, the $ZnCr_2O_4$ spinel might not be observed clearly by the XRD technique. For this reason, .the soils were spiked with ZnO and Cr_2O_3 to investigate the formation of spinel crystalline structure during thermal treatment of that matrix.

For the Zn- and Cr-enriched soil, the XRD patterns revealed that Zn and Cr incorporated successfully into the $ZnCr_2O_4$ spinel structure after thermal treatment at 1000°C (Fig. 7a). Besides the existence of the $ZnCr_2O_4$ as a predominant phase, quartz (SiO_2), as a major component in the soil, was also identified. The Zn leachability of both the sintered and un-sintered AZC samples was measured (Fig. 7b). The concentration of Zn leached from the un-sintered samples reached ~2300 mg/L, but a substantial decrease to 100 mg/L was observed after relatively low-temperature sintering (800°C). With further increase in the sintering temperature,

https://doi.org/10.1007/s42860-019-00053-w Published online by Cambridge University Press

the Zn concentration dropped to ~1 mg/L which is three orders lower than in the raw mixture. Therefore, even in the artificially contaminated soils with relatively large Zn and Cr contents, Zn was stabilized by the formation of $ZnCr_2O_4$ spinel after the relatively low-temperature thermal treatment.

The leachability of other heavy metals was also decreased dramatically in the brownfield soils after thermal treatment at 1000°C. Concentrations of Zn, Cr, Cu, Cd, Al, Fe, and Si were 2.38, 0.68, 1.39, 0.08 , 15.61, 0.40, 0.49 mg/L, respectively, in the leachates of the un-spiked, un-sintered soils. However, after thermal treatment, the corresponding concentrations were decreased to 0.31, 0.12, 0.16, 0.03, 1.26, 0.03, and 0.28 mg/L, respectively (Fig. 8). As implied by the study of the mechanism of incorporation of ZnO and Cr_2O_3 into the spinel structure, Zn acts as the divalent ions while Cr is trivalent. Therefore, $ZnCr_2O_4$ spinel will be generated during the sintering process, causing a significant reduction in metal leaching. Moreover, besides Cr(III), other major elemental components such as Al and Fe also exist in the reaction system in the trivalent state; thus enabling the incorporation of other hazardous, such as copper and zinc in the other spinel structures (such as $CuAl_2O_4$). With the successful stabilization of multiple heavy metals, contaminated brownfield soils can be used beneficially as part-substitution for clay minerals to produce a variety of ceramic products, such as bricks, refractories, and road pavement materials (Shih et al. 2006; Zhou & Keeling 2013; Smol et al. 2015; Zhou et al. 2016).

CONCLUSION

By combing advanced analytical technologies like XRD, XPS, TEM, and XANES, $ZnCr_2O_4$ spinel was identified in a sintered mixture of ZnO + Cr_2O_3, indicating the possibility of simultaneously incorporating divalent Zn and trivalent Cr in the spinel structure. 70.55% of available Zn was included in a $ZnCr_2O_4$ spinel phase at the lowest temperature used in this study (700°C). While the *TR* value of Zn increased continuously with increasing temperature until reaching nearly 100% at 1300°C, Zn leachability from the $ZnCr_2O_4$ phase was 170 times lower than from its oxide form over a long period of leaching. Moreover, Zn and Cr were also well stabilized in soils artificially enriched in Zn and Cr, with the $ZnCr_2O_4$ spinel as the predominant product phase. A concomitant significant decrease in zinc leachability was also observed in the sintered samples. In addition, sintering of the brownfield-site soils yielded excellent metal immobilization. The results of this study indicate that Zn and Cr are incorporated into a $ZnCr_2O_4$ phase when thermally treated at 1300°C, which provides a safe, reliable, and beneficial strategy to utilize the waste brownfield-site soils.

ACKNOWLEDGMENTS

This research was supported by the National Key Research and Development Program of China (2018YFC1801402), the Science and Technology Foundation of Guangdong, China (2016B020242006 and 2016TX03Z086), the Science and Technology Foundation of Guangzhou, China (201704020200 and 201804010197), the National Natural Science Foundations of China (U1701241, U1612442, and 21707063), and the Frontier Science Research Programme of CAS (QYZDB-SSW-DQC046).

REFERENCES

Basta, N. T., & McGowen, S. L. (2004). Evaluation of chemical immobilization treatments for reducing heavy metal transport in a smelter-contaminated soil. *Environmental Pollution, 127*, 73–82.

Bardos, R. P., Jones, S., Stephenson, I., Menger, P., Beumer, V., Neonato, F., Maring, L., Ferber, U., Track, T., & Wendler, K. (2016). Optimising value from the soft re-use of brownfield sites. *Science of The Total Environment, 563–564*, 769–782.

Bolan, N., Kunhikrishnan, A., Thangarajan, R., Kumpiene, J., Park, J., Makino, T., Kirkham, M. B., & Scheckel, K. (2014). Remediation of heavy metal(loid)s contaminated soils – to mobilize or to immobilize? *Journal of Hazardous Materials, 266*, 141–166.

Chen, S., Wu, Y., Cui, P., Chu, W., Chen, X., & Wu, Z. (2013). Cation distribution in $ZnCr_2O_4$ nanocrystals investigated by X-ray absorption fine structure spectroscopy. *Journal of Physical Chemistry C, 117*, 25019–25025.

Chen, Y., Hipel, K. W., Kilgour, D. M., & Zhu, Y. (2009). A strategic classification support system for brownfield redevelopment. *Environmental Modelling & Software, 24*, 647–654.

Capobianco, O., Costa, G., & Baciocchi, R. (2017). Assessment of the environmental sustainability of a treatment aimed at soil reuse in a brownfield regeneration context. *Journal of Industrial Ecology, 22*, 1027–1038.

Cameselle, C., & Gouveia, S. (2019). Phytoremediation of mixed contaminated soil enhanced with electric current. *Journal of Hazardous Materials, 361*, 95–102.

Coulon, F., Jones, K., Li, H., Hu, Q., Gao, J., Li, F., & Canning, K. (2016). China's soil and groundwater management challenges: lessons from the UK's experience and opportunities for China. *Environment International, 91*, 196–200.

De Kimpe, C. R., & Morel, J. (2000). Urban soil management: a growing concern. *Soil Science, 165*, 31–40.

Dermont, G., Bergeron, M., Mercier, G., & Richer-Laflèche, M. (2008). Soil washing for metal removal: A review of physical/chemical technologies and field applications. *Journal of Hazardous Materials, 152*, 1–31.

Dixit, T., Palani, I. A., & Singh, V. (2015). Investigation on the influence of dichromate ion on the ZnO nano-dumbbells and $ZnCr_2O_4$ nano-walls. *Journal of Materials Science: Materials in Electronics, 26*, 821–829.

Epling, W. S., Hoflund, G. B., Hart, W. M., & Minahan, D. M. (1997). Reaction and surface characterization study of higher alcoholsynthesis catalysts. *Journal of Catalysis, 169*, 438–446.

Fonseca, B., Figueiredo, H., Rodrigues, J., Queiroz, A., & Tavares, T. (2011). Mobility of Cr, Pb, Cd, Cu and Zn in a loamy sand soil: A comparative study. *Geoderma, 164*, 232–237.

Fu, F., Xie, L., Tang, B., Wang, Q., & Jiang, S. (2012). Application of a novel strategy–Advanced Fenton-chemical precipitation to the treatment of strong stability chelated heavy metal containing wastewater. *Chemical Engineering Journal, 189–190*, 283–287.

Gallagher, F. J., Pechmann, I., Bogden, J. D., Grabosky, J., & Weis, P. (2008). Soil metal concentrations and vegetative assemblage structure in an urban brownfield. *Environmental Pollution, 153*, 351–361.

Gene, S. A., Saion, E. B., Shaari, A. H., Kamarudeen, M. A., & Al-Hada, N. M. (2015). Fabrication and characterization of nano spinel $ZnCr_2O_4$ using thermal treatment method. *Advanced Materials Research, 1107*, 301–307.

Gingasu, D., Mindru, I., Culita, D. C., Patron, L., Calderon-Moreno, J. M., Preda, S., Oprea, O., Osiceanu, P., & Morena Pineda, E. (2014).

Investigation of nanocrystalline zinc chromite obtained by two soft chemical routes. *Materials Research Bulletin, 49*, 151–159.

Hsu, N., Wang, S., Lin, Y., Sheng, G. D., & Lee, J. (2009). Reduction of Cr(VI) by crop-residue-derived black carbon. *Environmental Science & Technology, 43*, 8801–8806.

Huynh, T., Tong, A. R., Singh, B., & Kennedy, B. J. (2003). Cd-substituted goethites – a structural investigation by synchrotron X-ray diffraction. *Clays and Clay Minerals, 51*, 397–402.

Kadir, A. A., Hassan, M. I. H., Salim, N. S. A., Sarani, N. A., Ahmad, S., & Rahmat, N. A. I. (2018). Stabilization of heavy metals in fired clay brick incorporated with wastewater treatment plant sludge: leaching analysis. *Journal of Physics: Conference Series, 995*, 1–10.

Kumpiene, J., Lagerkvist, A., & Maurice, C. (2008). Stabilization of As, Cr, Cu, Pb and Zn in soil using amendments–A review. *Waste Management, 28*, 215–225.

Lee, S., Lee, J., Jeong Choi, Y., & Kim, J. (2009). In situ stabilization of cadmium-, lead-, and zinc-contaminated soil using various amendments. *Chemosphere, 77*, 1069–1075.

Li, D., Li, R., Zhu, Z., Wu, X., Liu, F., Zhao, B., Cheng, J., & Wang, B. (2018). Elemental characteristics and paleoenvironment reconstruction: a case study of the Triassic lacustrine Zhangjiatan oil shale, southern Ordos Basin, China. *Acta Geochimica, 37*, 134–150.

Li, X., He, C., Bai, Y., Ma, B., Wang, G., & Tan, H. (2014). Stabilization/solidification on chromium (III). wastes by C_3A and C_3A hydrated matrix. *Journal of Hazardous Materials, 268*, 61–67.

Li, X., Liu, L., Wang, Y., Luo, G., Chen, X., Yang, X., Hall, M. H. P., Guo, R., Wang, H., Cui, J., & He, X. (2013). Heavy metal contamination of urban soil in an old industrial city (Shenyang) in Northeast China. *Geoderma, 192*, 50–58.

Lin, Y., & Wang, S. (2012). Chromium(VI) reactions of polysaccharide biopolymers. *Chemical Engineering Journal, 181–182*, 479–485.

Lombi, E., Zhao, F. J., Dunham, S. J., & McGrath, S. P. (2001). Phytoremediation of heavy metal–contaminated soils. *Journal of Environmental Quality, 30*, 1919–1926.

Lu, X., & Shih, K. (2012). Metal stabilization mechanism of incorporating lead-bearing sludge in kaolinite-based ceramics. *Chemosphere, 86*, 817–821.

Luo, X., Yu, S., Zhu, Y., & Li, X. (2012). Trace metal contamination in urban soils of China. *Science of the Total Environment, 421–422*, 17–30.

Mao, L., Cui, H., An, H., Wang, B., Zhai, J., Zhao, Y., & Li, Q. (2014). Stabilization of simulated lead sludge with iron sludge via formation of $PbFe_{12}O_{19}$ by thermal treatment. *Chemosphere, 117*, 745–752.

Marinković, Z., Mančić, L., Vulić, P., & Milošević, O. (2004). The influence of mechanical activation on the stoichiometry and defect structure of a sintered ZnO-Cr_2O_3 system. *Materials Science Forum, 453–454*, 423–428.

Mulligan, C. N., Yong, R. N., & Gibbs, B. F. (2001). Remediation technologies for metal-contaminated soils and groundwater: an evaluation. *Engineering Geology, 60*, 193–207.

Naumkin, A.V., Kraut-Vass, A., & Powell, C.J. (2008). NIST X-ray photoelectron spectroscopy database. Measurement Services Division of the National Institute of Standards and Technology (NIST). Technology Services.

Prabhukumar, G., Matsumoto, M., Mulchandani, A., & Chen, W. (2004). Cadmium removal from contaminated soil by tunable biopolymers. *Environmental Science & Technology, 38*, 3148–3152.

Sarıkaya, Y., Ada, K., & Önal, M. (2008). A model for initial-stage sintering thermodynamics of an alumina powder. *Powder Technology, 188*, 9–12.

Shih, K., White, T., & Leckie, J. O. (2006). Nickel stabilization efficiency of aluminate and ferrite spinels and their leaching behavior. *Environmental Science & Technology, 40*, 5520–5526.

Smol, M., Kulczycka, J., Henclik, A., Gorazda, K., & Wzorek, Z. (2015). The possible use of sewage sludge ash (SSA) in the construction industry as a way towards a circular economy. *Journal of Cleaner Production, 95*, 45–54.

Snellings, R. (2015). Surface chemistry of calcium aluminosilicate glasses. *Journal of the American Ceramic Society, 98*, 303–314.

Song, H., Laudenschleger, D., Carey, J. J., Ruland, H., & Nolan, M. (2017). Spinel-structured $ZnCr_2O_4$ with excess Zn is the active ZnO/Cr_2O_3 catalyst for high-temperature methanol synthesis. *ACS Catalysis, 7*, 7610–7622.

Stephen, S. E., Lawrence, L. M., Roy, R. A., & Wallace, W. D. (2007). Thermodynamics of Cr_2O_3, $FeCr_2O_4$, $ZnCr_2O_4$, and $CoCr_2O_4$. *The Journal of Chemical Thermodynamics, 39*, 1474–1492.

Su, M., Liao, C., Chan, T., Shih, K., Xiao, T., Chen, D., Kong, L., & Song, G. (2017). Incorporation of cadmium and nickel into ferrite spinel solid solution: XRD and EXAFS study. *Environmental Science & Technology, 52*, 775–782.

Su, M., Tang, J., Liao, C., Kong, L., Xiao, T., Shih, K., Song, G., Chen, D., & Zhang, H. (2018). Cadmium stabilization via silicates formation: Efficiency, reaction routes and leaching behavior of products. *Environmental Pollution, 239*, 571–578.

Sun, Y., Li, Y., Xu, Y., Liang, X., & Wang, L. (2015). In situ stabilization remediation of cadmium (Cd) and lead (Pb) co-contaminated paddy soil using bentonite. *Applied Clay Science, 105–106*, 200–206.

Tang, Y., Chan, S., & Shih, K. (2014). Copper stabilization in beneficial use of waterworks sludge and copper-laden electroplating sludge for ceramic materials. *Waste Management, 34*, 1085–1091.

Tang, Y., Chui, S. S., Shih, K., & Zhang, L. (2011a). Copper stabilization via spinel formation during the sintering of simulated copper-laden sludge with aluminum-rich ceramic precursors. *Environmental Science & Technology, 45*, 7609–7610.

Tang, Y., & Shih, K. (2014). Mechanisms of zinc incorporation in aluminosilicate crystalline structures and the leaching behavior of product phases. *Environmental Technology, 36*, 2977–2986.

Tang, Y., Shih, K., Li, M., & Wu, P. (2016). Zinc immobilization in simulated aluminum-rich waterworks sludge systems. *Procedia Environmental Sciences, 31*, 691–697.

Tang, Y., Shih, K., Wang, Y., & Chong, T. (2011b). Zinc stabilization efficiency of aluminate spinel structure and its leaching behavior. *Environmental Science & Technology, 45*, 10544–10550.

Tang, Y., Xin, X., Shih, K., & Wang, Z. (2018). Effect of crystal size on zinc stabilization in aluminum-rich ceramic matrix. *Journal of Material Cycles and Waste Management, 20*, 2110–2116.

Velasco, P. M., Ortíz, M. M., Giró, M. M., & Velasco, L. M. (2014). Fired clay bricks manufactured by adding wastes as sustainable construction material–A review. *Construction and Building Materials, 63*, 97–107.

Woetzel, J., Mendonca, L., Devan, J., Negri, S., Hu, Y., Jordan, L., Li, X., Maasry, A., Tsen, G., & Yu, F. (2009). *Preparing for China's urban billion*. McKinsey Global Institute.

Wuana, R. A., & Okieimen, F. E. (2011). Heavy metals in contaminated soils: A review of sources, chemistry, risks and best available strategies for remediation. *ISRN Ecology, 2011*, 1–20.

Yao, Z., Li, J., Xie, H., & Yu, C. (2012). Review on remediation technologies of soil contaminated by heavy metals. *Procedia Environmental Sciences, 16*, 722–729.

Zhou, C., & Keeling, J. (2013). Fundamental and applied research on clay minerals: From climate and environment to nanotechnology. *Applied Clay Science, 74*, 3–9.

Zhou, C., Zhao, L., Chen, T., & He, H. (2016). Current fundamental and applied research into clay minerals in China. *Applied Clay Science, 119*, 3–7.

Zhou, G., Yin, X., Zhou, J., & Cheng, W. (2017). Speciation and spatial distribution of Cr in chromite ore processing residue site, Yunnan, China. *Acta Geochimica, 36*, 1–7.

(Received 4 February 2019; revised 26 June 2019; AE: Chun-Hui Zhou)